THE JOURNAL OF PHYSICAL CHEMISTRY B

Article

pubs.acs.org/JPCB

The Regulatory Implications of Hydroquinone for the Multifunctional Enzyme Dehaloperoxidase-Hemoglobin from *Amphitrite ornata*

Jing Zhao, Junjie Zhao, and Stefan Franzen*

Department of Chemistry, North Carolina State University, Raleigh, North Carolina 27695, United States

Supporting Information

ABSTRACT: Hydroquinone (H_2Q) has been observed to compete with the oxidation of substrates 2,4,6-tribromophenol (2,4,6-TBP) and 2,4,6-trichlorophenol (2,4,6-TCP) catalyzed by the dehaloperoxidase-hemoglobin (DHP) from *Amphitrite ornata* in the presence of H_2O_2. This competition is observed as a lag phase during which H_2Q is preferentially oxidized to 1,4-benzoquinone (1,4-BQ) while totally inhibiting either 2,4,6-TBP or 2,4,6-TCP oxidation. The inhibition by H_2Q is distinct from that of the native competitive inhibitor 4-bromophenol (4-BP) since H_2Q is itself oxidized and its product 1,4-BQ is not an inhibitor. Thus, once H_2Q is completely consumed, the inhibition is removed, and normal substrate turnover is initiated, which explains the lag phase. To probe the mechanism of lag phase, the reactions between H_2Q and DHP were both studied both in the presence and in the absence of H_2O_2. The reversible reactions between ferric/oxyferrous DHP A and H_2Q/1,4-BQ are shown to involve a proton-coupled electron transfer (PCET) mechanism, where the distal histidine His^{55} serves as the proton acceptor. The pK_a of the distal histidine His^{55} has been determined by resonance Raman spectroscopy in order to corroborate its involvement in this mechanism. Consistent with the proposed mechanism, kinetic assays have shown that H_2Q serves as a substrate for DHP that follows the Michaelis–Menten kinetics. Unlike H_2Q, the product 1,4-BQ has a relatively large K_i value and therefore has negligible inhibition. This study sheds light on understanding the difference between substrate and inhibitor binding sites and regulatory implication for the peroxidase and oxygen-transporter functions in DHP. It also provides information on PCET in DHP, which is important for resolving the switching between the ferric peroxidase catalytic function and the ferrous oxygen transport function.

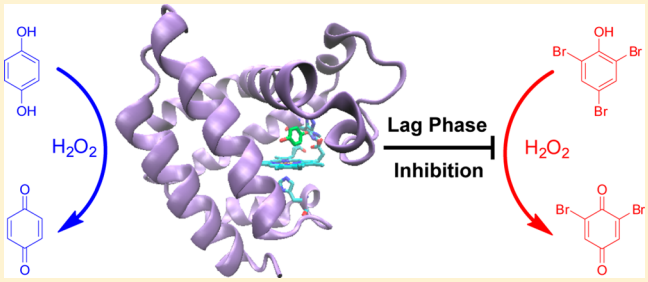

INTRODUCTION

Dehaloperoxidase-hemoglobin A (DHP A) is the first hemoglobin identified with a biologically relevant peroxidase function.[1] This multifunctional protein is structurally similar to sperm whale myoglobin (SWMb), but possesses more than 12-fold greater peroxidase activity toward the native substrate 2,4,6-TBP.[2] This unique peroxidase activity allows *Amphitrite ornata* to cohabit with *Notomastus lobatus* and other marine organisms that secrete highly toxic halogenated aromatic compounds.[1,3,4] Two isoforms of DHP have been discovered, in which DHP A and DHP B are distinguished by 5 out of 137 amino acids of monomer protein sequence.[5] Both isoforms are able to catalyze the oxidation of 2,4,6-trihalogenated phenol to form the 2,6-dihalogenated quinone in the presence of cosubstrate H_2O_2 (Scheme 1). Since the catalytic rate for oxidation of phenolic substrates by DHP B is 3 times faster than in DHP A, there is a clear indication that catalytic processes are important for the function of both of these globins.[6] Moreover, DHP A has been shown to have a sulfide oxidase activity,[7] which leads to the recognition that DHP is a multifunctional protein. We will refer to DHP as a general designation for any statement, which applies to both DHP A and DHP B.

Scheme 1. DHP-Catalyzed Oxidative Dehalogenation of TXP in the Presence of Cosubstrate H_2O_2

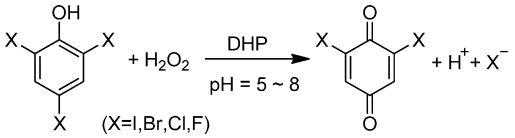

DHP A has been shown to possess distinct substrate and inhibitor binding sites in the distal pocket. 4-BP binds in the distal pocket perpendicular to the heme and serves as a nonclassical competitive inhibitor to DHP A.[8,9] The substrate 2,4,6-TBP binding site has been recently shown to have a binding site, which is buried even more deeply in the globin.[10] An additional two 2,4,6-TCP binding sites in the distal pocket have recently been discovered,[11] which causes us to pose the question: how many substrates can bind and how many modes of binding are there in this relatively small protein? The internal 2,4,6-TBP substrate binding site is located above the α-edge of

Received: August 1, 2013
Revised: October 8, 2013
Published: October 31, 2013

   dx.doi.org/10.1021/jp407663n | J. Phys. Chem. B 2013, 117, 14615–14624

the heme in the crystal structure, suggesting the functional possibility of internal oxidation by a sequential two-electron mechanism.[10] Consideration of the mechanism consistent with substrate binding must also include the role played by the distal histidine, which is His^{55} in DHP. The conserved distal histidine His^{55} of DHP, similar to that of myoglobin[12] and horseradish peroxidase (HRP),[13] has shown pH-dependent allosteric behavior which is believed to be both important for regulatory control and catalytic activation.[8,14−20]X-ray crystal structures have shown that the distal histidine His^{55} of DHP has much greater conformational flexibility than the distal histidine His^{64} of SWMb at pH 6.0.[14,16] The open conformation of His^{64} of SWMb is only observed at pH 4.0 while it is observed at pH 6.0 in DHP.[21] The distal histidine His^{55} has shown to be essential for functioning as an acid−base catalyst in facilitating the O−O heterolysis of H_2O_2,[16] resulting in formation of active oxidative species Compound ES, a ferryl species with an amino acid radical locates on the tyrosine Tyr^{38} or Tyr^{34}.[20,22]The compound ES label used in DHP A and B is attributed to an analogous compound ES intermediate formed in cytochrome c peroxidase (CcP), noting that the radical in CcP is located on tryptophan instead of on tyrosine.[23]

Although extensive studies have focused on the mechanism whereby DHP carries out peroxidase reactions and identification of the substrate binding sites, only recently has research begun to focus on understanding the mechanism of the interplay between the ferric and oxyferrous states of DHP with respect to peroxidase function.[24,25] This issue is central to DHP function since DHP mostly exists in the oxyferrous form *in vivo*. It is not known how DHP switches to a peroxidase function from a typical hemoglobin oxygen transport function. Previous studies have shown that DHP can initiate the peroxidase function from the oxyferrous state by a direct formation of the active ferryl species, Compound II, in the presence of substrate 2,4,6-TCP and cosubstrate H_2O_2,[6,26,27] providing an exceptional example that challenges the conventional peroxidase paradigm. The normal peroxidase reaction cycle starts and ends with the ferric heme Fe. For example, for HRP the cycle consists of Ferric HRP → Compound I → Compound II → Ferric HRP. The oxyferrous state is never produced in that cycle, and it is considered an inactive dead end in most peroxidases. The alternative cycle in DHP starts with oxyferrous DHP (DHP-O_2), DHP-O_2 → Compound II → Ferric DHP → DHP-O_2. Surprisingly, ferric DHP can be reduced back to the oxyferrous state (Ferric DHP → DHP-O_2) when exposed to the oxidation product 2,6-dichloroquinone (2,6-DCQ).[24] One can surmise that the role played by 2,6-DCQ would most likely be that of a redox mediator. Quinones are easily reduced to the hydroquinone, which is in turn an excellent reducing agent. This unorthodox role for the product, 2,6-DCQ, may become clearer once we understand electron transfer in DHP. However, the product 2,6-DCQ spontaneously reacts to form 3-hydroxy-2,6-dichloroquinone (3-OH-2,6-DCQ), which complicates the use of this reagent for studies of the electron transfer pathways in DHP.[28] The 2,6-dibromohydroquinone is also unstable and cannot be purchased. The benzoquinone/hydroquinone system is a more stable molecule for study of the role played by hydroquinones in the DHP mechanism. During the course of such studies an unusual kinetic role for benzohydroquinone was discovered.

Herein, we report the unique kinetic behavior of benzohydroquinone (H_2Q) on the DHP reaction cycle. Indeed, H_2Q can reduce DHP from the ferric to the ferrous form. However, studies of enzymatic activity using 2,4,6-TCP as the substrate led to an usual observation of a "lag phase" for the catalytic oxidation of substrate by DHP A. The lag phase differs from an inhibitory process in that there is no measurable product (2,6-DCQ) formed until H_2Q is completely consumed. At the end of the lag phase, turnover begins and the 2,6-DCQ product forms at a normal rate, i.e. similar to the rate observed in the presence of H_2O_2 but without any H_2Q. In order to elucidate the mechanism of lag phase, both the interactions of H_2Q with DHP A in the absence and in the presence of H_2O_2 must be considered. It is highly relevant for the previous suggestion of a role for 2,6-DBQ that H_2Q reversibly reduces ferric DHP A to the oxyferrous state by a proton-coupled electron transfer (PCET) mechanism facilitated by the distal histidine His^{55}, where the distal histidine His^{55} not only stabilizes the bound O_2 ligand by hydrogen bonding but also serves as a proton acceptor during reduction of the heme by H_2Q. A pH-dependent distal histidine conformational behavior has been measured in both ferric and oxyferrous states. A complete thermodynamic scheme of proton and electron transfer has been established by applying resonance Raman spectroscopy combined with previously measured electrochemistry data. The binding site of H_2Q was probed by an inhibition assay with the standard inhibitor 4-bromophenol (4-BP). Given the unique functional range of DHP, this study provides further insights into the difference between substrate and inhibitor binding sites, as well as the interplay between initiation of peroxidase function from the ferric state or the oxyferrous state. Such functional considerations are at the heart of any study of multifunctional proteins since they show how different functions are regulated and how they can be mutually tolerated in a single protein.

MATERIAL AND METHODS

Materials. All reagents were purchased from Aldrich and ACROS and used without further purification. 2,4,6-Trichlorophenol (2,4,6-TCP), 2,4,6-tribromophenol (2,4,6-TBP), and 4-bromophenol (4-BP) were each dissolved in 100 mM, pH = 7.0 potassium phosphate (KP_i) buffer to prepare the stock solution. H_2Q and 1,4-BQ were prepared by a direct weighing method in the 100 mM KP_i buffer at desired pH. Prepared solutions were stored at 4 °C and protected against light. Other concentrations were measured by monitoring their absorbance: 1,4-BQ, $\varepsilon_{246\ nm}$ = 20,600 M^{-1} cm^{-1}; TCP, $\varepsilon_{312\ nm}$ = 3752 M^{-1} cm^{-1}; TBP, $\varepsilon_{316\ nm}$ = 4640 M^{-1} cm^{-1}; 4-BP, $\varepsilon_{280\ nm}$ = 1370 M^{-1} cm^{-1}. Spectra were obtained using an Agilent 8453 diode array UV−visible spectrophotometer with a Peltier-cooled sample cell at 25 °C. Hydrogen peroxide solution was freshly made before each kinetic experiment and kept on ice and protected against light during the experiment. Wild-type His6X (histidine-tagged) DHP A and H55D mutant were expressed in *E. coli* and purified as previously described.[16,29] The concentration of both ferric and oxyferrous DHP A was determined by using the molar absorption coefficient, ε = 116,400 M^{-1} cm^{-1}.[30] Oxyferrous DHP was prepared by adding excess amount of sodium dithionite ($Na_2S_2O_4$) to the purified ferric DHP. Then the solution was filtered through the PD-10 column to get rid of the remaining $Na_2S_2O_4$ and bubbled with oxygen for 5 min.

Bench-Top Mixing Kinetic Assays. The kinetic assays were conducted using an Agilent 8453 UV−visible spectrophotometer operating in kinetic mode with a 1 s time resolution.

dx.doi.org/10.1021/jp407663n | J. Phys. Chem. B 2013, 117, 14615−14624

The catalytic reactions were carried out in a 0.4 cm path length cuvette obtained from Starna Cells, Inc. with a total volume of 1200 μL. The ferric DHP A concentration $[E]_0$ in each sample was 2.4 μM. For the reaction in the absence of H_2O_2 DHP A and KP_i buffer were first mixed and allowed to incubate for 3 min in a cuvette placed in the thermal cell to reach thermal equilibrium. Subsequently, 200 μL of substrate solution was added into the cuvette to initiate the reaction. For the reaction in the presence of H_2O_2, the substrate H_2Q were first mixed with ferric DHP A and KP_i buffer and then allowed to incubate for 3 min in the cuvette placed in the thermal cell to let DHP A fully reduced to oxyferrous and to reach thermal equilibrium at the same time. Subsequently, 200 μL of 7.2 mM H_2O_2 solution was added into the cuvette to initiate the reaction. The kinetic data were measured by monitoring the absorbance at wavelength 246 nm, which corresponds to the absorbance peak of the 1,4-BQ, with a molar absorption coefficient $\varepsilon_{246\ nm}$ = 20,600 M^{-1} cm^{-1}.

Stopped-Flow UV−Visible Kinetic Assays. Experiments were performed on a Bio-Logic SFM-400 triple-mixing stopped-flow instrument equipped with a diode array UV−visible spectrophotometer and were carried out at 23 °C in 100 mM KP_i buffer, pH 7.0. Data were collected over three time-domain regimes (2.5, 25, and 250 ms; 300 scans each) using the Bio Kinet32 software package (Bio-Logic). Data were collected (900 scans total) over a three-time domain regime (2.5, 25, and 250 ms; 300 scans each, 83.25 s total). Single−mixing experiments were performed, in which ferric DHP A were preincubated with H_2Q prior to the mixing with H_2O_2. The final concentration after mixing were [DHP A] = 5 μM, $[H_2Q]$ = 55 μM, $[H_2O_2]$ = 500 μM.

Resonance Raman Spectroscopy. DHP A samples at a final protein concentration of 100 μM were prepared in 100 mM KP_i buffer, pH 7. 0. Samples were placed in 5 mm NMR tubes and spun with an air piston spinning sample holder (Princeton Photonics, model Raman 101). Resonance Raman spectra were obtained by excitation at the edge of the Soret band at 410 nm using a Coherent Mira 900 tunable titanium sapphire laser generating 700−1000 nm light. The Ti:sapphire laser was pumped by a Coherent Verdi 10 frequency-doubled diode-pumped Nd:vanadate laser that generated 10 W of 532 nm light. The near-IR output from the Ti:sapphire laser was sent through a Coherent 5-050 frequency doubler to generate the working range of 400−430 nm light for Soret band excitation. The frequency doubled beam was collimated and cylindrically focused to a vertical line of ~5 mm and typically 45−60 mW at the sample. Raman scattered light was collected by the Spex 1877 Triplemate monochromator (2400 grooves/mm final stage grating) and was detected by a liquid N_2-cooled CCD camera (ISA Spex, model CCD-3000). Spectra were measured at room temperature for 40 acquisitions with total exposure time of 1200 s. The spectra were calibrated using standard spectra of toluene and carbon tetrachloride.

Data Analysis. For reaction between ferric DHP A and H_2Q and the reverse reaction between oxyferrous DHP A and 1,4-BQ, the time-resolved spectra measured in the benchtop kinetic assay were analyzed using the singular value decomposition (SVD) method. SVD provides a decomposition of the original absorption data matrix $\mathbf{A}(\lambda,t)$ in terms of basis spectra as the product of three matrices $\mathbf{USV}^T$. The $\mathbf{V}^T$ matrix (Figures S2 and S5 in Supporting Information [SI]), corresponding to the time-course evolution, was evaluated as a one step irreversible first-order reaction and globally fitted to a single exponential function $A = c_0 + c_1 \exp(-k_{obs}t)$, from which the apparent rate constant k_{obs} and $\mathbf{C}$ matrix were determined. The spectra corresponding to each reaction species were calculated based on the analytical solution of the one-step irreversible first-order reaction model (SI). The SVD and global fitting analysis were performed using Igor Pro 6.0.

The kinetic data for the DHP A-catalyzed oxidation of H_2Q in the presence of H_2O_2, were fitted using the short time approximation. The slope of experimental progress curve was determined by linear fit of the first 10 time points to provide the initial rates V_0. A series of initial rates V_0 obtained as a function of the substrate concentration were then fitted to the Michaelis−Menten equation to obtain the parameters V_{max} and K_m (Table 1).

Table 1. Michaelis-Menten Kinetic Parameters for Oxidation of H_2Q by DHP A

T/K	k_{cat} (s^{-1})	K_m (μM)	k_{cat}/K_m (10^{-3} s^{-1} M^{-1})
303	0.450 ± 0.008	59.7 ± 5.8	7.53 ± 0.74
298	0.280 ± 0.007	65.3 ± 8.0	4.29 ± 0.53
293	0.216 ± 0.003	87.5 ± 5.1	2.47 ± 0.15
288	0.138 ± 0.003	75.1 ± 7.8	1.84 ± 0.19

The pH-dependent Raman spectra were first baseline subtracted by using a 4 point 4 polynomial extrapolation and normalized according to the intensity of the ν_4 band. Then the data matrix $\mathbf{A}(\tilde{\nu}, pH)$ was decomposed into three matrices $\mathbf{USV}^T$ using SVD method. The second eigen vectors of $\mathbf{V}^T$ matrix were fitted to the proposed model (Schemes S1, S2 in SI) in order to determine the corresponding pK_a value.

RESULTS

The Lag Phase Observed in the Catalytic Oxidation of 2,4,6-TCP. Figure 1 shows the oxidation kinetics of 2,4,6-TCP in the presence of H_2Q. Observation at 273 nm monitors the formation of the product 2,6-DCQ, while 246 nm monitors the oxidation of H_2Q. Figure 1 shows that no 2,6-DCQ product is formed during the first 25 s of the experiment. Instead, H_2Q is oxidized for a period of 25 s under the assay conditions of Figure 1. We call this delay in the formation of product, the lag phase. A lag phase is observed for both 2,4,6-TCP and the native substrate of DHP A 2,4,6-TBP. A key observation is that the duration of the lag phase depends linearly on the

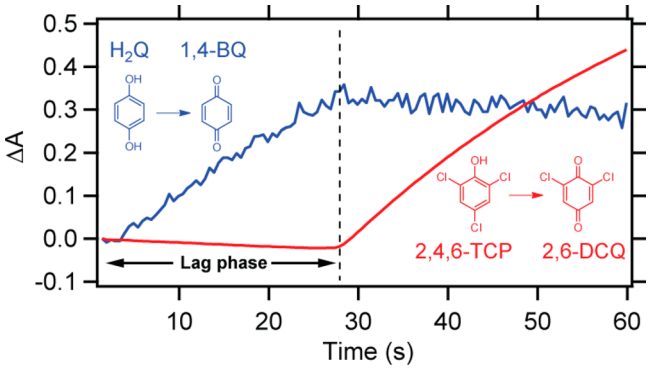

Figure 1. The lag phase of DHP A catalyzed oxidation of 2,4,6-TCP in the presence of H_2Q. The blue time course represents the turnover of H_2Q that forms 1,4-BQ, the red time course represents the turnover of 2,4,6-TCP that yields 2,6-DCQ.

dx.doi.org/10.1021/jp407663n | J. Phys. Chem. B 2013, 117, 14615−14624

Scheme 2. Reversible Reaction between Ferric DHP A with H_2Q and Oxyferrous DHP A with 1,4-BQ

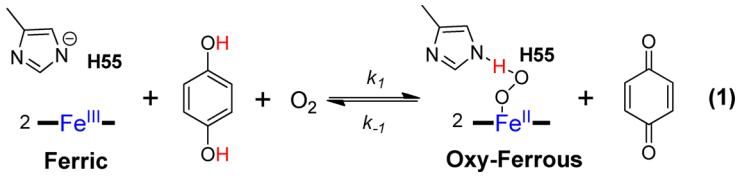

concentration of H_2Q added to the assay mixture (Figure S1 in SI). Since H_2Q reacts to form 1,4-BQ in the presence of DHP A (Scheme 2), one can surmise that the lag phase ends when H_2Q is consumed. One possible explanation for the lag phase is a reaction between H_2Q and ferric DHP A that is rapid compared to turnover of either 2,4,6-TCP or 2,4,6-TBP. In this case, H_2Q could completely block enzymatic turnover if it is bound inside the protein in the distal pocket in the inhibitor binding site.[8] However, this inhibition mechanism is satisfactory only if the binding of 1,4-BQ is weak compared to the binding of H_2Q. To test this two-part hypothesis we have studied the reduction of ferric DHP A by H_2Q and the competition between H_2Q and the native inhibitor 4-BP for the inhibitor binding site in the distal pocket. We also studied the binding constant for the product of H_2Q oxidation, 1,4-BQ.

The Reversible Reaction between Reduction of Ferric DHP A by H_2Q and Oxidation of Oxyferrous DHP A by 1,4-BQ. The time-resolved spectra (Figure S2 in SI) show that ferric DHP A has been reduced to the oxyferrous form while H_2Q has been oxidized to 1,4-BQ, characterized by an increase in absorbance at 246 nm. A well-defined isosbestic point can be observed throughout the reaction time course, indicating only one product has formed in this reaction. The SVD analysis of the spectra, shown in Figure 2, shows the initial spectrum in red

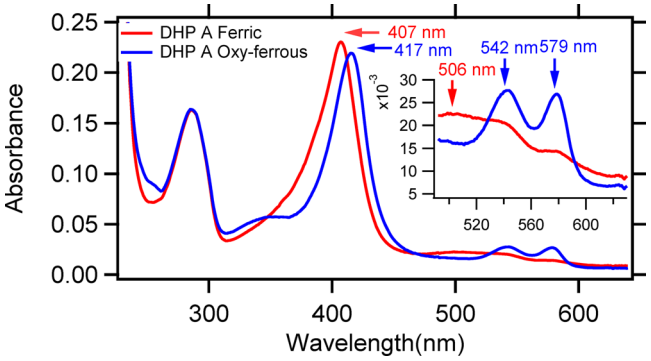

Figure 2. Reconstructed spectra of the reaction between ferric DHP A (red) and H_2Q that forms the oxyferrous DHP A (blue). (Inset) Expansion of the Q-band region.

with a Soret band at 407 nm and Q-band at 506 nm both belonging to the metaquo high spin ferric form of DHP A. The second spectrum shown in blue corresponds to the end point of the treatment with H_2Q. The blue spectrum in Figure 2 has a sharper red-shifted Soret band at 416 nm and the α,β branches of Q-band at 542 and 579 nm, both of which indicate the formation of six coordinated low-spin oxyferrous DHP A.

The reduction of ferric DHP A by H_2Q exhibits pseudo-first-order kinetics in the presence of at least 10-fold excess of H_2Q. The pseudo-first-order rate constant k_{obs} shows a linear dependence on $[H_2Q]$ (Figure 3). Thus, the second-order rate constant $k_1 = (2.21 \pm 0.04) \times 10^2\ M^{-1}s^{-1}$ can be obtained according to the expression $k_{obs} = k_1[H_2Q]$. Additionally, for the

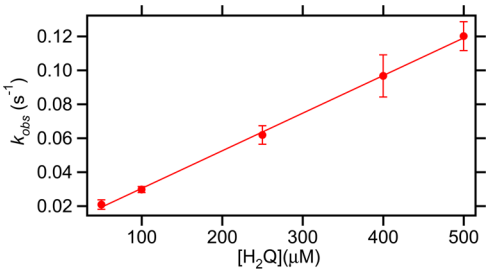

Figure 3. Plot of the k_{obs} vs $[H_2Q]$ for the reduction of ferric DHP A (5 μM) by H_2Q in 100 mM KP$_i$ buffer, pH 7.0 at 298 K.

reverse reaction, the oxidation of oxyferrous DHP A also follows pseudo-first-order kinetics in the presence of at least 10-fold excess of 1,4-BQ. The second order rate constant $k_{-1} = (7.35 \pm 0.25) \times 10^2\ M^{-1}s^{-1}$ (Figure S8 in SI). Thus, the equilibrium constant K_1 for this reversible reaction is $K_1 = k_1/k_{-1} = 3.32 \pm 0.11$.

The pH dependence of the second-order rate constant k_1 has been studied in the pH range from 5.0 to 8.0 (Figure S4 in SI). k_1 is stable below pH 6.5 and rapidly increases above pH 6.5. However, the oxidation at pH = 8.0 no longer follows first-order reaction kinetics. Although the H_2Q oxidation rate increases with pH, the effect is limited by the formation of hydroxy ferric DHP, which has a pK_a = 8.1. Thus at pH = 8.0, approximately 50% of the ferric DHP has been ligated with hydroxide.[31] The axial hydroxide ligand prevents the outer-sphere electron transfer from H_2Q to the heme iron, thus inhibits the reduction of the protein.

$$\frac{k'_{obs}}{k_{obs}} = \frac{K_i}{K_i + [I]} \qquad (1)$$

It is not straightforward to directly measure a putative binding of H_2Q in the distal pocket since it reacts with ferric DHP A. However, we can probe whether H_2Q binds in the inhibitor binding site using a competitive binding assay with the inhibitor 4-BP, which has been established in inhibition assays of 2,4,6-TCP.[8] Consistent with the hypothesis that H_2Q binds in the distal pocket, the inhibitor 4-BP also acts to inhibit the reduction of the heme iron in the presence of H_2Q. It is known that inhibitor 4-BP binds in the distal pocket of DHP A with binding affinity K_d =1.15 mM in the metaquo resting state measured by resonance Raman spectra at room temperature.[8] The value under conditions of turnover is K_i = 0.155 mM as measured by an inhibition kinetic assay at 298K.[32] The kinetic assays show that the rate of heme reduction by H_2Q decreases in the presence of 4-BP (Figure 4). A plausible hypothesis for this inhibition behavior is that both H_2Q and 4-BP compete for the same internal binding site. Since 4-BP is not reactive in the distal pocket it inhibits the oxidation of H_2Q. The inhibition data have been fitted to eq 1, resulting in K_i = 0.283 mM at 298 K. The discrepancy between two K_i values measured in two sets of kinetic assays is due to the different kinetic assay conditions.

dx.doi.org/10.1021/jp407663n | J. Phys. Chem. B 2013, 117, 14615−14624

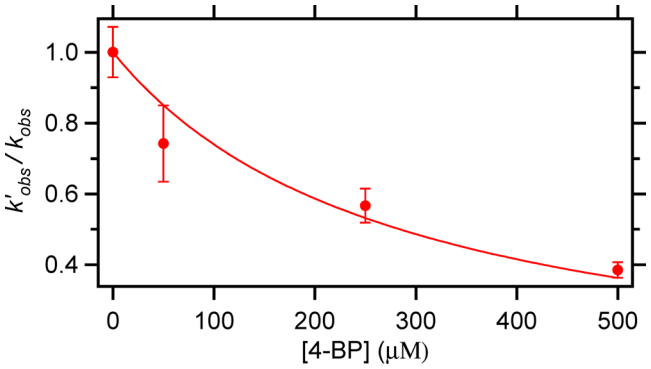

Figure 4. Inhibitor 4-BP inhibits reduction of ferric DHP A by H_2Q. The reaction mixture consists of 5 μM Ferric DHP A reacting with 500 μM H_2Q in the presence of 0, 50, 250, 500 μM 4-BP in 100 mM KP_i buffer, pH 7.0 at 298 K.

Previously, K_i was measured in the presence of cosubstrate H_2O_2 under turnover conditions, whereas K_i is measured in the absence of H_2O_2 in this experiment.

The temperature dependence of second-order constant k_1 for the oxidation of H_2Q by ferric DHP A has been studied at 283, 288, 293, and 298 K. ln (k_1) vs $1/T$ has been plotted according to the Eyring equation (eq 2) to obtain the thermodynamic parameters $\Delta H^{\ddagger} = 20.0 \pm 1.4$ kJ/mol, $\Delta S^{\ddagger} = -132 \pm 5$ J/(mol K), which gives the Gibbs free energy for the transition state $\Delta G^{\ddagger} = 59.4 \pm 2.9$ kJ/mol (Figure 5).

$$\ln \frac{k}{T} = \ln \frac{k_B}{h} + \frac{\Delta S^{\ddagger}}{R} - \frac{\Delta H^{\ddagger}}{RT} \qquad (2)$$

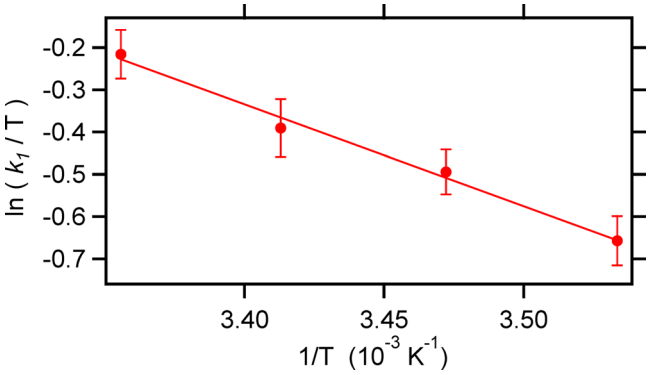

Figure 5. Eyring plot for the oxidation of H_2Q by ferric DHP A (5 μM) in 100 mM KP_i buffer, pH 7.0.

Distal Histidine His^{55} Acts As a Proton Acceptor Facilitating the Oxidation of H_2Q by a Proton Coupled Electron Transfer (PCET) Mechanism. The distal histidine His^{55} has been shown to be essential for the oxidation of H_2Q by DHP A. For example, the ferric DHP A mutant H55D has no detectable activity toward H_2Q oxidation. The pK_a values for the distal histidine His^{55} have been measured in both ferric and oxyferrous forms by resonance Raman spectroscopy. The allosteric behavior of His^{55} is crucial in controlling the coordination state of the heme iron in a pH-dependent manner. In the ferric metaquo state, the distal histidine favors the closed conformation that stabilizes the distal water ligand at high pH, whereas it swings out of the distal pocket into the solvent and favors the open conformation at low pH. As a consequence, the coordination and spin state of heme iron switch from 6-coordinate high spin (6cHS) to 5-coordinate high spin (5cHS). This trend can be clearly seen in the resonance Raman spectra as function of pH shown in Figure 6.

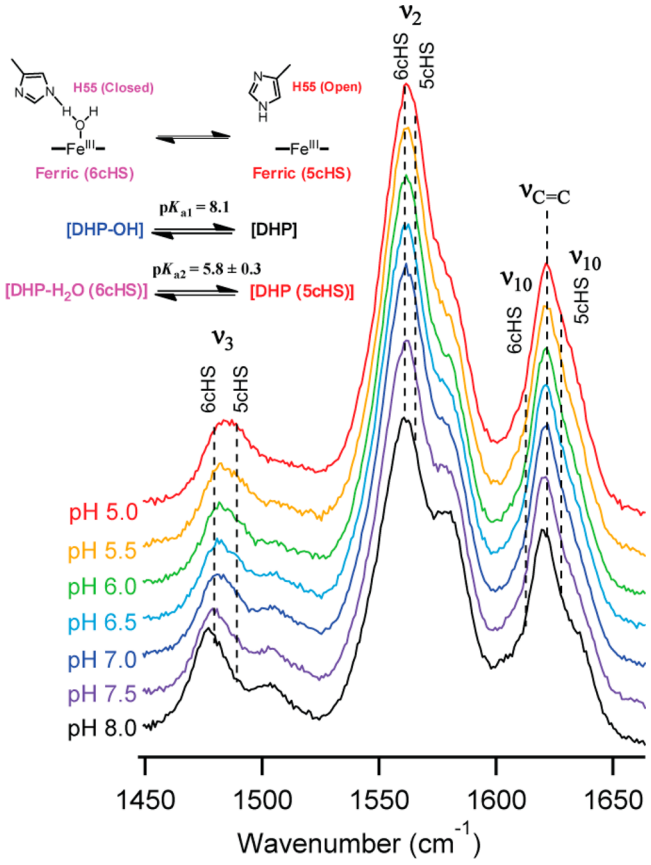

Figure 6. Resonance Raman spectra of metaquo DHP A as a function of pH in the high frequency region. A scheme describing the relevant equilibra for ferric DHP A is shown in the figure .

The population of 5cHS gradually shifts to 6cHS as the pH rises. However, when pH is above 7.5, the rapid increase of the population of 6cHS is due to the formation of hydroxide ligated form. The acid/alkaline transition in DHP A has been previously measured with a pK_a = 8.1.[31] Thus, a dual equilibrium model with different pK_a values (pK_{a1} = 8.1) is used to fit the population curve obtained from SVD analysis. The analysis gives pK_a = 5.8 ± 0.3 for the distal histidine His^{55} in ferric DHP (Figure 6).

In the oxyferrous form, the distal histidine His^{55} forms a hydrogen bond to the dioxygen in the closed conformation. This hydrogen bond significantly increases the oxygen binding affinity of DHP in a way that is similar to other hemoglobins.[33] At low pH, this hydrogen bond is disrupted due to the open conformation of the histidine.[15] Although the conformation of the distal histidine is changed upon a pH shift, this does not result in deligation of O_2. Thus, the measurement of the conformation change of His^{55} using resonance Raman spectroscopy would have been challenging or impossible if were not for a light-induced oxidation of DHP A. It happens coincidentally that the autoxidation rate of oxyferrous DHP A is dramatically accelerated by laser photoexcitation, which provides a method for estimating the population ratio between closed and open conformations of oxyferrous DHP A. It is

dx.doi.org/10.1021/jp407663n | J. Phys. Chem. B 2013, 117, 14615−14624

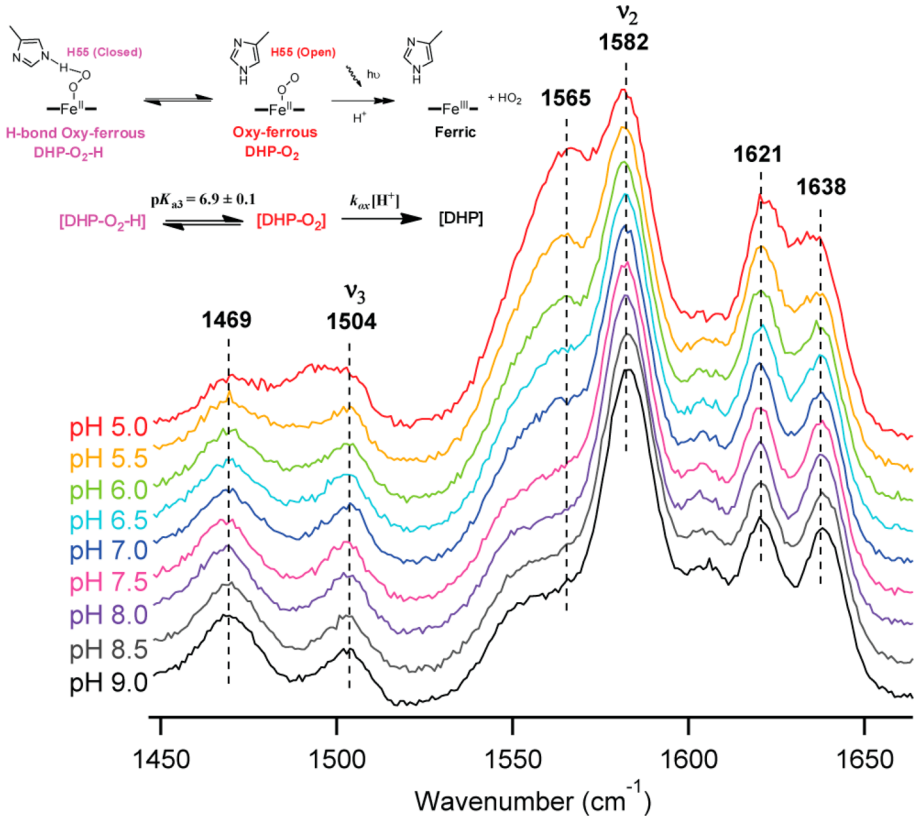

Figure 7. Resonance Raman spectra of oxyferrous DHP A as a function of pH in the high-frequency region. A photoexcitation reaction scheme for deoxyferrous DHP A is shown in Figure.

hypothesized that only the oxyferrous form of DHP A with distal histidine His^{55} in the open conformation will be excited due to the lack of hydrogen bond stabilization to the dioxygen ligand. Upon photoexcitation, oxyferrous DHP without hydrogen bond is oxidized into the ferric state. The photoexcited autoxidation has also shown a pH-dependent manner, in which the autoxidation rate is much faster at low pH, probably attributed to the formation of a protonated superoxide species (Figure 7). Thus, an equilibrium model combined with photoexcited autoxidation conversion was proposed and fitted to the population curve obtained from SVD analysis. Using this method, the pK_a of the distal histidine His^{55} in oxyferrous DHP A was determined to be 6.9 ± 0.1 (see SI).

The redox potential between $Fe^{(III)}/Fe^{(II)}$ in the anaerobic condition at pH 7.0 has been measured to be $E°$ = 0.221 V.[34] Under aerobic conditions, the redox potential between $Fe^{(III)}/Fe^{(II)}$-O_2 is about 0.08 V higher than the value measured in the anaerobic condition, $E°$ = 0.305 V, due to the binding of O_2 to the heme iron that stabilizes the ferrous state Fe and changes the d electrons from high spin to low spin.[34] The pK_a values for the protein matrix of both ferric and oxyferrous DHP A that take up or expel a proton have been measured using the resonance Raman spectrophotometric method. A thermodynamic cycle shown in Scheme 3 can be established on the basis of these data. The bond dissociation free energy (BDFE) of **Fe^{II}-O_2~His^{55}-H** can be calculated from both routes, either starting from proton transfer (PT), BDFE (**Fe^{II}-O_2~His^{55}-H**) = 5.73 pK_a + 96.48 $E°$ + C_G = 303.8 ± 1.7 kJ/mol (C_G is a solvent constant, as for water, C_G = 241.16 kJ/mol)[35] or electron transfer (ET), BDFE (**Fe^{II}-O_2~His^{55}-H**) = 302.0 ± 0.6 kJ/mol. According to Hess' law, the energy change should

Scheme 3. Thermodynamic Scheme of Proton and Electron Transfer of Fe^{II}-O_2~His^{55}-H

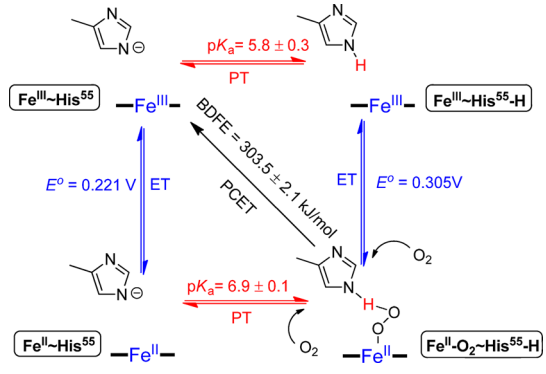

be independent of the path; thus, the consistency between these two BDFE (**Fe^{II}-O_2~His^{55}-H**) supports the validity of the two pK_a values measured by resonance Raman spectroscopy. Moreover, as for reaction 1, $\Delta G°$ = BDFE (**Fe^{II}-O_2~His^{55}-H**) − BDFE (H_2Q) = $-RT \ln K_1$. Since the average BDFE (H_2Q) = 307.5 kJ/mol in aqueous solution[35] and K_1 = 3.32 ± 0.11, BDFE (**Fe^{II}-O_2~His^{55}-H**) can be calculated to be 304.5 ± 0.1 (298K). The BDFE (**Fe^{II}-O_2~His^{55}-H**) calculated from the reversible reaction equilibrium constant is within error of the value predicted from thermodynamic square scheme.

DHP A Catalyzed Oxidation of H_2Q in the Presence of H_2O_2. In order for H_2Q to act catalytically in place of 2,4,6-TBP during the lag phase, it must be oxidized by H_2O_2. Yet, H_2Q will reduce the heme and thus, any catalytic role for DHP must involve a ferrous, rather than ferric heme. The question of

dx.doi.org/10.1021/jp407663n | J. Phys. Chem. B 2013, 117, 14615−14624

whether H_2Q can be catalytically oxidized by DHP A was addressed using similar methods employed for the substrates, 2,4,6-TCP and 2,4,6-TBP (see Table 2). The time-resolved

Table 2. Michaelis–Menten Kinetic Parameters of DHP A Substrates

Substrate	k_{cat} (s^{-1})	K_M (mM)	$E_a(k_{cat})$ (kJ/mol)	$E_a(k_{cat}/K_M)$ (kJ/mol)
H_2Q	0.28	0.065	55.2	69.3
2,4,6-TBP (10% MeOH)	1.55	0.713	47.9	45.5
2,4,6-TCP	7.16	1.08	44.0	56.3

spectrum shows that DHP A starts in the oxyferrous state after incubating with H_2Q for 3 min. Once H_2O_2 is added, DHP A is observed to be in the oxyferrous state after incubating with H_2Q for 3 minutes as shown in Figure 8. The Soret band shifts

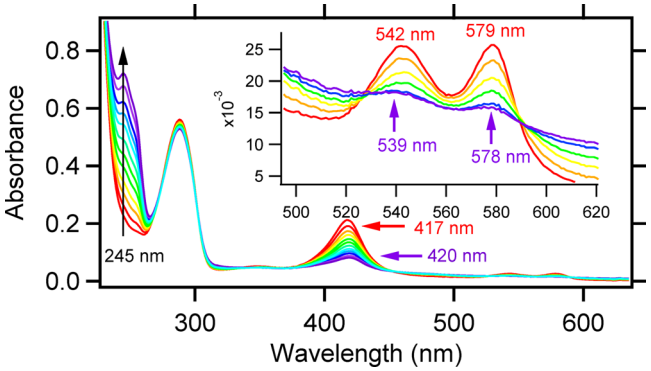

Figure 8. Time-resolved spectrum of DHP catalytic oxidation of H_2Q in the presence of H_2O_2 (From red to purple). The subwindow shows the scale up of Q-band region. The kinetic assay conditions are 5 μM DHP reacting with 500 μM H_2Q in the presence of 1200 μM H_2O_2 in100 mM KP_i buffer at 298 K.

from 417 to 420 nm, α and β branches of the Q-band decrease in intensity Figure 8. The rising peak at 245 nm is attributed to the formation of product, 1,4-BQ. No ferric DHP intermediate was observed during the reaction time course in the much higher time resolution of the stopped-flow kinetic assay (Figures S14, S15 in SI), suggesting that the activation of oxyferrous DHP undergoes a concerted two-electron oxidation yielding compound II, and then is reduced by substrate hydroquinone in a direct two-electron reduction.

The oxidation of H_2Q catalyzed by DHP A in the presence of H_2O_2 follows Michaelis–Menten kinetics as shown in Figure 9. The kinetic parameters k_{cat} and K_m were obtained by fitting the curve of the initial rate to the Michaelis–Menten equation (Figure 9). The temperature dependence of k_{cat} and K_m were obtained by conducting the kinetic measurement at four temperatures, 288, 293, 298, and 303 K. The Arrhenius plot gives activation energy E_a = 69.3 ± 7.4 kJ/mol for k_{cat}/K_m, and E_a = 55.2 ± 4.3 kJ/mol for k_{cat}.

The pH dependence of the initial rate for H_2Q in this reaction is similar to that of 2,4,6-TCP. At low pH, the initial rate is faster; however, DHP A undergoes a competing deactivation reaction to form compound RH.[20,22,36] Thus, the total amount of product that is eventually produced is actually less than that at pH 7.0. The pH dependence of the initial rate can be fitted into the sigmoid curve with a midpoint value at pH = 6.13 ± 0.08.

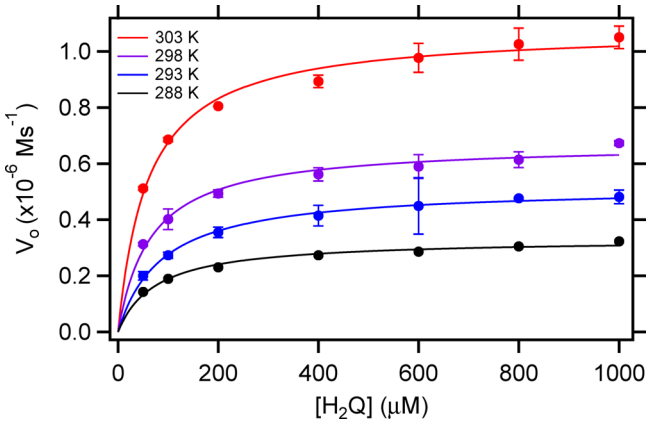

Figure 9. Michaelis–Menten kinetics of catalytic oxidation of H_2Q by DHP A. The kinetic assays were conducted using 2.4 μM DHP A to react with varying concentrations of H_2Q in the presence of 1200 μM H_2O_2 in 100 mM KP_i buffer, pH 7.0 at 303 K (red), 298 K (purple), 293 K (blue), 288 K (black).

DISCUSSION

The lag phase caused by H_2Q in the catalytic oxidation of 2,4,6-TCP by DHP A presents an intriguing question about the substrate specificity of DHP A. H_2Q acts as an extraordinarily potent inhibitor of the oxidation of 2,4,6-TCP, while it is simultaneously oxidized to 1,4-BQ. 2,4,6-TCP starts to turn over only after H_2Q has been completely consumed. The duration of the lag phase is proportional to the amount of the H_2Q in the solution mixture. Thus, one can quantitatively substantiate that H_2Q leads to the lag phase.

The Oxidation of H_2Q by Ferric DHP A in the Absence of H_2O_2 by a PCET Mechanism. The reaction between ferric DHP A and H_2Q involves a net H^+ and e^- transfer from the substrate H_2Q to ferric DHP A. In principle, there are three pathways, in which this reaction can take place. The H^+ and e^- are either transferred by a concerted step by a PCET mechanism, or they undergo separate proton transfer (PT) and electron transfer (ET) reactions. Since the thermodynamic diagrams of H_2Q, $HQ^\bullet$ (Scheme S3 in SI), and $\mathbf{Fe^{II}\text{-}O_2\sim His^{55}\text{-}H}$ (Scheme 3) have all been established, the thermodynamic analysis provides a basic argument to examine the possible reaction pathways.

For the reaction between ferric DHP A and H_2Q, the activation energy between transition state and ground state obtained by the Eyring plot gives $\Delta G^{\ddagger}$ = 59.4 ± 2.9 kJ/mol.

Therefore,

(a) For the initial ET and subsequent PT process:

$$\Delta G^{\circ}_{ET} = -(96.48\ \text{kJ mol}^{-1}\ \text{V}^{-1}) \times (0.221 - 1.10)$$
$$= 84.80\ \text{kJ mol}^{-1}$$

The free energy is much higher than that of activation energy; thus, this pathway is not possible.

(b) As for the initial PT and subsequent PT process:

$$\Delta G^{\circ}_{PT} = -(5.73\ \text{kJ mol}^{-1}) \times (5.8 - 9.85)$$
$$= 23.21\ \text{kJ mol}^{-1}$$

Thus, the initial proton process cannot be ruled out by the thermodynamic argument. However, forming an anion in the highly hydrophobic distal pocket requires a

dx.doi.org/10.1021/jp407663n | J. Phys. Chem. B 2013, 117, 14615–14624

Scheme 4. Proposed Mechanism of the Lag Phase Due to the Presence of H_2Q

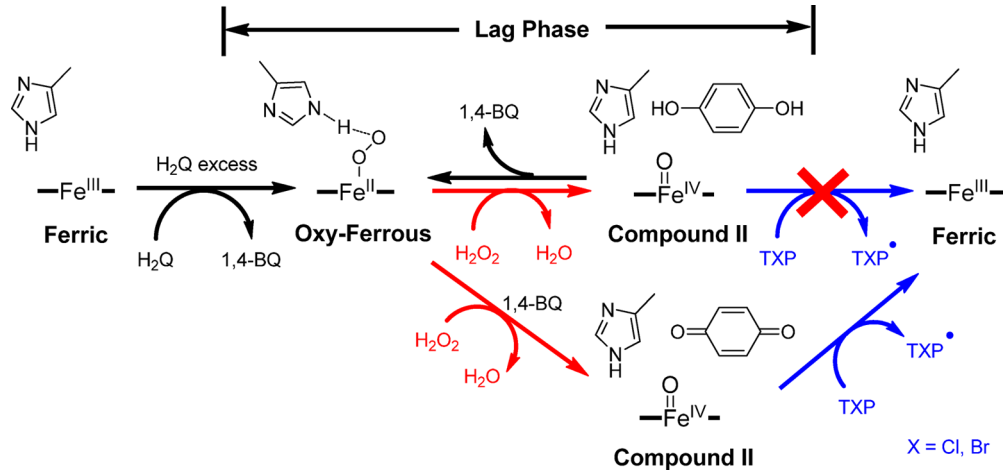

large amount of solvation energy. Thus, this pathway is also very unlikely.

(c) PCET describes a process that ET and PT will take place simultaneously, resulting in a lower free energy for the whole process.

$$\Delta G^{\circ}_{PCET} = -(5.73\ \text{kJ mol}^{-1})(5.8 - 9.85) + (96.48\ \text{kJ mol}^{-1}\ \text{V}^{-1}) \times (0.46 - 0.305) = 38.16\ \text{kJ mol}^{-1}$$

PCET mechanism transfers the $1H^+$ and $1e^-$ in a single kinetic step, circumvents the high-energy intermediates, resulting in a significantly lower activation energy.[37]

The reactions between H_2Q and several transition metal complexes have been shown to undergo a PCET mechanism.[38−40] One example that has a resemblance to DHP A is an iron protoporphyrin IX model compound that reacts with H_2Q in a separate PCET mechanism, in which the electron acceptor and proton acceptor are far apart. In the iron protoporphyrin IX model compound, the heme iron accepts the electron, whereas the propionate group serves as the proton acceptor.[41] Although DHP A contains a similar prosthetic group heme *b*, compared to the iron protoporphyrin IX model compound, our study shows that DHP A utilizes the distal histidine His^{55} as a proton acceptor. Thus, we conclude that the reaction between H_2Q and ferric DHP A also undergoes a separated PCET mechanism. The distance between N_ε of distal histidine His^{55} to the heme iron is 4.8 Å in the closed conformation as measured in the wild-type DHP A X-ray crystal structure.[15] The distal histidine His^{55} has been shown to be essential for catalysis in DHP A. For example, the H55D mutant, which replaces histidine with aspartate mutant, has 10-fold lower reactivity,[16] and the H55 V mutant has no measurable catalytic activity.[42] The distal histidine, His^{55}, serves as the proton acceptor in the PCET transfer mechanism only when it maintains the closed conformation. Protonation of His^{55} causes it to rotate out into the solvent-exposed open conformation. Thus, there is a tight coupling of His^{55} with the function of DHP A. The central role of His^{55} in catalysis and protection has been discussed in a number of studies.[8,16,19,20] This work suggests that His^{55} could be important as well in the electron transfer reaction required to complete the reaction cycle.

The Oxidation of H_2Q by DHP and the Connection to the Lag Phase. The catalytic reactions carried out by ferric DHP A follow a reaction cycle similar to CcP. Normal peroxidase chemistry consists activation of the ferric state by binding of H_2O_2 to form the high valent active species Compound ES and Compound II, which are the initial active intermediates formed in HRP[43] and CcP,[23] respectively. Subsequently, substrate is oxidized in two one-electron oxidations and the heme is reduced back to the ferric state by these electrons, which enables it to carry out another catalytic cycle (Scheme 4). However, due to its very high reduction potential, DHP A can perform chemistry that is not possible for the other members of the peroxidase family. Specifically, DHP A and B can initiate the peroxidase reactions starting from the oxyferrous state. In fact, the oxyferrous state has been shown to be as competent as the ferric state as the starting point of peroxidase reaction catalyzed by DHP.[24] Since H_2Q reduces ferric heme to the oxyferrous state, it would inactivate most peroxidases, but it does not have this effect on DHP. Furthermore, a reductant of some kind is essential in order to complete the oxyferrous peroxidase cycle shown in Scheme 4. It is possible that the observed behavior of H_2Q is analogous to the native reductant, which may even involve transient hydroquinone formation by 2,6-DBQ. Thus, the finding of this study may have relevance for native behavior. Since DHP has a native oxygen transport function it is reasonable to suppose that DHP A initiates peroxidase chemistry from the oxyferrous state *in vivo* and that the reactions observed here are analogous to native reduction chemistry.

Besides acting a reductant as shown in Scheme 4, H_2Q plays an additional role as an inhibitor. H_2Q is oxidized to 1,4-BQ in the process of reducing oxyferrous DHP A to form the ferryl species compound II. The inhibition of this process by 4-BP is consistent with the hypothesis that H_2Q binds in the inhibitor site in the distal pocket. The observed greater affinity for 4-BP is consistent with the trend in the 4-halophenols, which have increasing dissociation constants in the order 4-FP > 4-CP > 4-BP > 4-IP. H_2Q is sterically closest to 4-CP, which means it should be displaced by 4-BP, as observed. If this model is correct, then the inhibition of 2,4,6-TBP will persist in the presence of H_2Q until it is completely consumed by catalytic oxidation in the presence of H_2O_2. This behavior would give rise to the observed lag phase since only after all of the H_2Q has

dx.doi.org/10.1021/jp407663n | J. Phys. Chem. B 2013, 117, 14615−14624

been converted to 1,4-BQ, can 2,4,6-TBP begin to be catalytically oxidized. Consistent with the proposed role for H_2Q, 1,4-BQ was shown to be a very poor inhibitor, since its K_i is ~3.91 mM (Figures S16 and S17 in SI). Thus, its inhibition effect can be ignored and DHP A returns to a normal peroxidase cycle. As expected from the lag phase kinetics, the magnitude of k_{cat}/K_m for H_2Q is in slightly greater than k_{cat}/K_m for the native substrate. On the basis of our data, we find that k_{cat}/K_m for H_2Q is ~4.3 mM s^{-1}, which is intermediate between 2,4,6-TBP and 2,4,6-TCP, for which k_{cat}/K_m is ~2.0 and ~6.6 mM s^{-1}, respectively.

The hypothesis that H_2Q binds in the 4-BP (inhibitor) binding site in the distal pocket is consistent with steric interactions that are known in the distal pocket of DHP. Based on the inhibition of H_2Q oxidation by 4-BQ one would conclude both 4-BQ and H_2Q compete for the same internal binding site. Although the binding of H_2Q in the inhibitor site is inhibitory for 2,4,6-TCP or 2,4,6-TBP turnover, that same site can serve as an active site for H_2Q since it is activated for oxidation by electron transfer. Moreover, the hydroxyl group of H_2Q bound in the inhibitor site is immediately in contact with the heme near His^{55} and leading to the possibility of rapid PCET. We have shown elsewhere that the inhibitor binding site is different from the 2,4,6-TBP substrate binding site[10] and a recent study reveals two more binding sites for 2,4,6-TCP in the distal pocket, which are distinct from the inhibitor binding site.[11] Binding of substrate in any of these sites is excluded by binding of a molecule in the inhibitor site. Thus, we find that H_2Q binding in the inhibitor site provides a consistent explanation for the experimental observations, although it is still not proven conclusively.

In summary, the present study establishes that H_2Q plays a unique role in the chemistry of DHP. We initiated this study in order to understand whether the reduction of the DHP would complete the catalytic cycle and thereby resolve the functional paradox that arises from activation of an oxyferrous protein for peroxidase chemistry. In order to complete the reaction cycle there must be a reducing agent that returns DHP to the oxyferrous state. The present study shows that a hydroquinone has the potential to play the role of a reducing agent that completes the catalytic cycle. Moreover, the possibility of PCET suggests an alternative activation pathway in DHP that would involve reduction of bound O_2 as it occurs in oxygenases and oxidases. The functional complexity of dehaloperoxidase-hemoglobin continues to provide interesting examples of the role that multifunctional proteins can play in marine ecosystems.

■ ASSOCIATED CONTENT

Supporting Information

SVD analysis and subsequent model construction, derivation and fitting are presented. This material is available free of charge via the Internet at http://pubs.acs.org.

■ AUTHOR INFORMATION

Corresponding Author

*E-mail: franzen@ncsu.edu

Notes

The authors declare no competing financial interest.

■ ACKNOWLEDGMENTS

This work was supporting by ARO Grant LS-58761. We thank Dr. Reza Ghiladi for helpful discussions and usage of the stopped-flow UV−visible spectrophotometer.

■ REFERENCES

(1) Chen, Y. P.; Woodin, S. A.; Lincoln, D. E.; Lovell, C. R. An Unusual Dehalogenating Peroxidase from the Marine Terebellid Polychaete Amphitrite ornata. *J. Biol. Chem.* **1996**, *271* (9), 4609−12.

(2) Belyea, J.; Gilvey, L. B.; Davis, M. F.; Godek, M.; Sit, T. L.; Lommel, S. A.; Franzen, S. Enzyme Function of the Globin Dehaloperoxidase from Amphitrite ornata is Activated by Substrate Binding. *Biochemistry* **2005**, *44* (48), 15637−15644.

(3) Lincoln, D. E.; Fielman, K. T.; Marinelli, R. L.; Woodin, S. A. Bromophenol Accumulation and Sediment Contamination by the Marine Annelids Notomastus Lobatus and Thelepus Crispus. *Biochem. Syst. Ecol.* **2005**, *33* (6), 559−570.

(4) Roach, M. P.; Chen, Y. P.; Woodin, S. A.; Lincoln, D. E.; Lovell, C. R.; Dawson, J. H. Notomastus Lobatus Chloroperoxidase and Amphitrite Ornata Dehaloperoxidase both Contain Histidine as their Proximal Heme Iron Ligand. *Biochemistry* **1997**, *36* (8), 2197−2202.

(5) Han, K.; Woodin, S. A.; Lincoln, D. E.; Fielman, K. T.; Ely, B. Amphitrite ornata, a Marine Worm, Contains Two Dehaloperoxidase Genes. *Mar. Biotechnol. (NY)* **2001**, *3* (3), 287−92.

(6) D'Antonio, J.; D'Antonio, E. L.; Thompson, M. K.; Bowden, E. F.; Franzen, S.; Smirnova, T.; Ghiladi, R. A. Spectroscopic and Mechanistic Investigations of Dehaloperoxidase B from Amphitrite ornata. *Biochemistry* **2010**, *49* (31), 6600−6616.

(7) Nicoletti, F. P.; Thompson, M. K.; Franzen, S.; Smulevich, G. Degradation of Sulfide by Dehaloperoxidase-Hemoglobin from Amphitrite ornata. *J. Biol. Inorg. Chem.* **2011**, *16* (4), 611−9.

(8) Thompson, M. K.; Davis, M. F.; de Serrano, V.; Nicoletti, F. P.; Howes, B. D.; Smulevich, G.; Franzen, S. Internal Binding of Halogenated Phenols in Dehaloperoxidase-Hemoglobin Inhibits Peroxidase Function. *Biophys. J.* **2010**, *99* (5), 1586−1595.

(9) de Serrano, V.; Franzen, S. Structural Evidence for Stabilization of Inhibitor Binding by a Protein Cavity in the Dehaloperoxidase-Hemoglobin from Amphitrite ornata. *Pept. Sci.* **2012**, *98* (1), 27−35.

(10) Zhao, J.; de Serrano, V.; Zhao, J. J.; Le, P.; Franzen, S. Structural and Kinetic Study of an Internal Substrate Binding Site in Dehaloperoxidase-Hemoglobin A from Amphitrite ornata. *Biochemistry* **2013**, *52* (14), 2427−2439.

(11) Wang, C.; Lovelace, L. L.; Sun, S.; Dawson, J. H.; Lebioda, L. Complexes of Dual-Function Hemoglobin/Dehaloperoxidase with Substrate 2,4,6-Trichlorophenol Are Inhibitory and Indicate Binding of Halophenol to Compound I. *Biochemistry* **2013**, *52* (36), 6203−6210.

(12) Phillips, G. N.; Arduini, R. M.; Springer, B. A.; Sligar, S. G. Crystal-Structure of Myoglobin from a Synthetic Gene. *Proteins: Struct., Funct., Genet.* **1990**, *7* (4), 358−365.

(13) Gajhede, M.; Schuller, D. J.; Henriksen, A.; Smith, A. T.; Poulos, T. L. Crystal Structure of Horseradish Peroxidase C at 2.15 Angstrom Resolution. *Nat. Struct. Biol.* **1997**, *4* (12), 1032−1038.

(14) Chen, Z.; De Serrano, V.; Betts, L.; Franzen, S. Distal Histidine Conformational Flexibility in Dehaloperoxidase from Amphitrite ornata. *Acta Crystallogr., Sect. D* **2009**, *65*, 34−40.

(15) de Serrano, V.; Chen, Z. X.; Davis, M. F.; Franzen, S. X-ray Crystal Structural Analysis of the Binding Site in the Ferric and Oxyferrous Forms of the Recombinant Heme Dehaloperoxidase Cloned from Amphitrite ornata. *Acta Crystallogr., Sect. D* **2007**, *63*, 1094−1101.

(16) Zhao, J.; de Serrano, V.; Dumarieh, R.; Thompson, M.; Ghiladi, R. A.; Franzen, S. The Role of the Distal Histidine in H_2O_2 Activation and Heme Protection in both Peroxidase and Globin Functions. *J. Phys. Chem. B* **2012**, *116* (40), 12065−77.

(17) Smirnova, T. I.; Weber, R. T.; Davis, M. F.; Franzen, S. Substrate Binding Triggers a Switch in the Iron Coordination in

Dehaloperoxidase from Amphitrite ornata: HYSCORE Experiments. *J. Am. Chem. Soc.* **2008**, *130* (7), 2128-+.
(18) Franzen, S.; Thompson, M. K.; Ghiladi, R. A. The Dehaloperoxidase Paradox. *Biochim. Biophys.-Proteins Proteom.* **2012**, *1824* (4), 578−588.
(19) Nicoletti, F. P.; Thompson, M. K.; Howes, B. D.; Franzen, S.; Smulevich, G. New Insights into the Role of Distal Histidine Flexibility in Ligand Stabilization of Dehaloperoxidase-Hemoglobin from Amphitrite ornata. *Biochemistry* **2010**, *49* (9), 1903−12.
(20) Thompson, M. K.; Franzen, S.; Ghiladi, R. A.; Reeder, B. J.; Svistunenko, D. A. Compound ES of Dehaloperoxidase Decays via Two Alternative Pathways Depending on the Conformation of the Distal Histidine. *J. Am. Chem. Soc.* **2010**, *132*, 17501−17510.
(21) Yang, F.; Phillips, G. N. Crystal Structures of CO-, Deoxy- and Met-myoglobins at Various pH Values. *J. Mol. Biol.* **1996**, *256* (4), 762−774.
(22) Feducia, J.; Dumarieh, R.; Gilvey, L. B. G.; Smirnova, T.; Franzen, S.; Ghiladi, R. A. Characterization of Dehaloperoxidase Compound ES and Its Reactivity with Trihalophenols. *Biochemistry* **2009**, *48* (5), 995−1005.
(23) Goodin, D. B.; Mauk, A. G.; Smith, M. Studies of the Radical Species in Compound ES of Cytochrome-C Peroxidase Altered by Site-Directed Mutagenesis. *Proc. Natl. Acad. Sci. U.S.A.* **1986**, *83* (5), 1295−1299.
(24) D'Antonio, J.; Ghiladi, R. A. Reactivity of Deoxy- and Oxyferrous Dehaloperoxidase B from Amphitrite ornata: Identification of Compound II and Its Ferrous Hydroperoxide Precursor. *Biochemistry* **2011**, *50* (27), 5999−6011.
(25) Du, J.; Sono, M.; Dawson, J. H. Functional Switching of Amphitrite ornata Dehaloperoxidase from O_2-Binding Globin to Peroxidase Enzyme Facilitated by Halophenol Substrate and H_2O_2. *Biochemistry* **2010**, *49* (29), 6064−6069.
(26) Davydov, R.; Osborne, R. L.; Kim, S. H.; Dawson, J. H.; Hoffman, B. M. EPR and ENDOR Studies of Cryoreduced Compounds II of Peroxidases and Myoglobin. Proton-Coupled Electron Transfer and Protonation Status of Ferryl Hemes. *Biochemistry* **2008**, *47* (18), 5147−55.
(27) Davydov, R.; Osborne, R. L.; Shanmugam, M.; Du, J.; Dawson, J. H.; Hoffman, B. M. Probing the Oxyferrous and Catalytically Active Ferryl States of Amphitrite ornata Dehaloperoxidase by Cryoreduction and EPR/ENDOR Spectroscopy. Detection of Compound I. *J. Am. Chem. Soc.* **2010**, *132* (42), 14995−5004.
(28) Franzen, S.; Sasan, K.; Sturgeon, B. E.; Lyon, B. J.; Battenburg, B. J.; Gracz, H.; Dumariah, R.; Ghiladi, R. Nonphotochemical Base-Catalyzed Hydroxylation of 2,6-Dichloroquinone by H_2O_2 Occurs by a Radical Mechanism. *J. Phys. Chem. B* **2012**, *116* (5), 1666−1676.
(29) Ma, H.; Thompson, M. K.; Gaff, J.; Franzen, S. Kinetic Analysis of a Naturally Occurring Bioremediation Enzyme: Dehaloperoxidase-Hemoglobin from Amphitrite ornata. *J. Phys. Chem. B* **2010**, *114* (43), 13823−9.
(30) Osborne, R. L.; Taylor, L. O.; Han, K. P.; Ely, B.; Dawson, J. H. Amphitrite ornata Dehaloperoxidase: Enhanced Activity for the Catalytically Active Globin using MCPBA. *Biochem. Biophys. Res. Commun.* **2004**, *324* (4), 1194−8.
(31) Nienhaus, K.; Deng, P.; Belyea, J.; Franzen, S.; Nienhaus, G. U. Spectroscopic Study of Substrate Binding to the Carbonmonoxy form of Dehaloperoxidase from Amphitrite ornata. *J. Phys. Chem. B* **2006**, *110* (26), 13264−76.
(32) Zhao, J.; Franzen, S. Kinetic Study of the Inhibition Mechanism of Dehaloperoxidase-Hemoglobin A by 4-Bromophenol. *J. Phys. Chem. B* **2013**, *117* (28), 8301−8309.
(33) Tsai, A.-L.; Berka, V.; Martin, E.; Olson, J. S. A "Sliding Scale Rule" for Selectivity among NO, CO, and O_2 by Heme Protein Sensors. *Biochemistry* **2011**, *51* (1), 172−186.
(34) D'Antonio, E. L.; Chen, T. K.; Turner, A. H.; Santiago-Capeles, L.; Bowden, E. F. Voltammetry of Dehaloperoxidase on Self-Assembled Monolayers: Reversible Adsorptive Immobilization of a Globin. *Electrochem. Commun.* **2013**, *26*, 67−70.
(35) Warren, J. J.; Tronic, T. A.; Mayer, J. M. Thermochemistry of Proton-Coupled Electron Transfer Reagents and Its Implications. *Chem. Rev.* **2010**, *110* (12), 6961−7001.
(36) Franzen, S.; Gilvey, L. B.; Belyea, J. L. The pH Dependence of the Activity of Dehaloperoxidase from Amphitrite ornata. *Biochim. Biophys. Acta-Proteins Proteom.* **2007**, *1774* (1), 121−130.
(37) Hammes-Schiffer, S. Theory of Proton-Coupled Electron Transfer in Energy Conversion Processes. *Acc. Chem. Res.* **2009**, *42* (12), 1881−1889.
(38) Binstead, R. A.; Mcguire, M. E.; Dovletoglou, A.; Seok, W. K.; Roecker, L. E.; Meyer, T. J. Oxidation of Hydroquinones by $[(Bpy)_2(Py)Ru(IV)(O)]^{2+}$ and $[(Bpy)_2(Py)Ru(III)(OH)]^{2+}$ - Proton-Coupled Electron-Transfer. *J. Am. Chem. Soc.* **1992**, *114* (1), 173−186.
(39) Song, N.; Gagliardi, C. J.; Binstead, R. A.; Zhang, M. T.; Thorp, H.; Meyer, T. J. Role of Proton-Coupled Electron Transfer in the Redox Interconversion between Benzoquinone and Hydroquinone. *J. Am. Chem. Soc.* **2012**, *134* (45), 18538−18541.
(40) Lam, W. W. Y.; Lee, M. F. W.; Lau, T. C. Kinetics and Mechanism of the Oxidation of Hydroquinones by a *trans*-Dioxoruthenium(VI) Complex. *Inorg. Chem.* **2006**, *45* (1), 315−321.
(41) Warren, J. J.; Mayer, J. M. Proton-Coupled Electron Transfer Reactions at a Heme-Propionate in an Iron-Protoporphyrin-IX Model Compound. *J. Am. Chem. Soc.* **2011**, *133* (22), 8544−8551.
(42) Franzen, S.; Belyea, J.; Gilvey, L. B.; Davis, M. F.; Chaudhary, C. E.; Sit, T. L.; Lommel, S. A. Proximal Cavity, Distal Histidine, and Substrate Hydrogen-Bonding Mutations Modulate the Activity of Amphitrite ornata Dehaloperoxidase. *Biochemistry* **2006**, *45* (30), 9085−9094.
(43) Miller, V. P.; Goodin, D. B.; Friedman, A. E.; Hartmann, C.; Demontellano, P. R. O. Horseradish-Peroxidase Phe(172)-]Tyr Mutant - Sequential Formation of Compound-I with a Porphyrin Radical-Cation and a Protein Radical. *J. Biol. Chem.* **1995**, *270* (31), 18413−18419.